Inversion of spinning sound fields

Michael Carley[a)]
Department of Mechanical Engineering, University of Bath, Bath BA2 7AY, England

(Received 30 September 2008; revised 24 November 2008; accepted 24 November 2008)

A method is presented for the reconstruction of rotating monopole source distributions using acoustic pressures measured on a sideline parallel to the source axis. The method requires no *a priori* assumptions about the source other than that its strength at the frequency of interest varies sinusoidally in azimuth on the source disk so that the radiated acoustic field is composed of a single circumferential mode. When multiple azimuthal modes are present, the acoustic field can be decomposed into azimuthal modes and the method applied to each mode in sequence. The method proceeds in two stages, first finding an intermediate line source derived from the source distribution and then inverting this line source to find the radial variation in source strength. A far-field form of the radiation integrals is derived, showing that the far-field pressure is a band-limited Fourier transform of the line source, establishing a limit on the quality of source reconstruction, which can be achieved using far-field measurements. The method is applied to simulated data representing wind-tunnel testing of a ducted rotor system (tip Mach number of 0.74) and to control of noise from an automotive cooling fan (tip Mach number of 0.14), studies which have appeared in the literature of source identification. © *2009 Acoustical Society of America.* [DOI: 10.1121/1.3050311]

PACS number(s): 43.28.We, 43.50.Nm, 43.20.Rz [AH] Pages: 690–697

I. INTRODUCTION

This paper describes a method for determining rotating source distributions from acoustic measurements. This is a problem which has been examined by a number of researchers, with many [1–6] considering the problem of estimating the amplitudes of the acoustic modes at the termination of a circular duct, as in the case of aircraft engines. The motivation for these studies has usually been to determine the source terms in their own right in order to find the source mechanisms responsible for the noise or to improve noise control measures, but a second application has been in developing models which can be used to predict the acoustic field. This prediction model can be used in active noise control[7,8] or in using near-field measurements taken in a wind tunnel to make far-field predictions of noise radiated by aircraft in flight.[1,9] This gives rise to two different, though related, problems: the first is the determination, to within some tolerance, of the acoustic source; the second is the determination of the acoustic source to within a tolerance sufficient to give accurate predictions of the acoustic field at points other than the measurement positions.

This paper considers a model problem for the recovery of a rotating source distribution from a set of measurements along a sideline, a line parallel to the source axis. The question of how to position microphones, and how many to use, features in the analysis of many researchers. Typical microphone configurations have included 3 microphones at 120 angular positions,[1] 91 microphones on a fixed polar array,[6] 18 microphones rotating over 20 positions,[2] and 21 microphones located on a fixed arc,[4] depending on the experimental facilities used and the fidelity of results required. Recent work on engine noise has also included the use of sensor arrays mounted inside or on the engine. Examples are the use of 100 pressure sensors on the surface of the intake[10] and simulations of an array of 150 microphones mounted on the wall of an engine duct.[11] In these cases, the methods used are described as "beamforming" and come from the class of techniques used for source location rather than for source characterization.

In this paper, we present an inversion technique which uses data from a linear arrangement of microphones to recover the details of a distribution of monopoles on a disk. This corresponds to the problem of thickness noise of a propeller or other rotors,[12] sound from a baffled circular piston[13] or to sound radiated by the termination of a circular duct, when the Rayleigh approximation is valid.[14,15] The only assumption made is that the source and the acoustic field have a known sinusoidal variation in azimuth—no assumption is required about the form of the radial variation of the source nor is a far-field approximation needed. The resulting method is applied to simulated data using parameters characteristic of problems to which identification methods have been applied in the past.

The source recovery technique which is developed here is based on the measurement techniques used in wind-tunnel measurement of aerodynamic sources[1–9] but could also be viewed in the more general framework of sound source reconstruction in other areas of acoustics[16] and, in particular, in relation to cylindrical near-field acoustical holography (NAH)[17,18] where measurements are taken on a cylindrical surface surrounding a source region and then forward projected to find the acoustic field elsewhere in space or back-projected to find the acoustic quantities which characterize the source. The method of this paper shares some similarities with NAH but differs in incorporating known information about the source geometry and azimuthal dependence.

[a)]Electronic mail: m.j.carley@bath.ac.uk

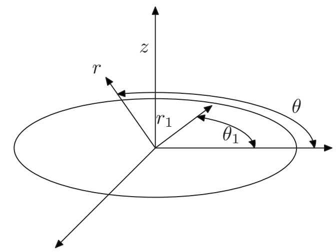

FIG. 1. Coordinate system for radiation prediction.

II. INVERSION OF SPINNING SOUND FIELDS

The acoustic fields to be considered in this paper can all be viewed as being generated by sources distributed over a disk. Figure 1 shows the arrangement of the problem. We use cylindrical coordinates (r, θ, z) with an acoustic monopole source distributed over the disk, $0 \leqslant r \leqslant 1$, $z=0$, nondimensionalizing all lengths on a disk radius. At a single frequency ω, the acoustic field p is given by[12]

$$p(r,\theta,z,\omega) = \int_0^1 \int_0^{2\pi} s(r_1,\theta_1)\frac{e^{ikR}}{4\pi R} d\theta_1 r_1 dr_1, \qquad (1)$$

with wavenumber $k=\omega/c$, c the speed of sound, and source-observer distance

$$R^2 = r^2 + r_1^2 - 2rr_1 \cos(\theta - \theta_1) + z^2.$$

The source term $s(r_1, \theta_1)$ can be decomposed into a series of azimuthal modes with sinusoidal variation,

$$s(r_1,\theta_1) = \sum_{n=-\infty}^{\infty} s_n(r_1) e^{jn\theta_1},$$

which, upon insertion into Eq. (1) with the transformation $\theta - \theta_1 \rightarrow \theta_1$, yields

$$p(r,\theta,z,\omega) = \sum_{n=-\infty}^{\infty} e^{jn\theta} \int_0^1 \int_0^{2\pi} s_n(r_1)\frac{e^{j(kR-n\theta_1)}}{4\pi R} d\theta_1 r_1 dr_1, \qquad (2)$$

with R being redefined,

$$R^2 = r^2 + r_1^2 - 2rr_1 \cos \theta_1 + z^2.$$

The acoustic field at a frequency ω is thus a sum of azimuthal modes, each of which is directly generated by a corresponding azimuthal mode on the source disk. The aim of the inversion procedure is to recover the source function(s) $s_n(r_1)$ given as input some acoustic pressures measured in the field. The nature of these measurements will depend on the type of source being studied.

There are two main categories of problem which will be considered: rotating sources such as propellers and fans and ducted sources where the duct termination can be considered a disk-shaped source. For a source rotating at angular frequency Ω, the radiated field contains only harmonics of frequency $n\Omega$. Furthermore, if the source strength is steady in the rotating reference frame, there is only one azimuthal mode, of order n, present at each of these frequencies. This means that the acoustic field of Eq. (2) reduces to

$$p(r,\theta,z,n\Omega) = e^{jn\theta} \int_0^1 \int_0^{2\pi} s_n(r_1)\frac{e^{j(kR-n\theta_1)}}{4\pi R} d\theta_1 r_1 dr_1.$$

The properties of the acoustic field are largely controlled by the rotor speed and, in particular, the tip Mach number, which, for a source of unit radius, is $M_t=\Omega/c$. When the source rotates supersonically, $M_t > 1$, the acoustic field is dominated by the source around the sonic radius $r^* = 1/M_t$.[19] When $M_t < 1$, the blade tip is the dominant region, and in the far field, its radiation is exponentially stronger than that from inboard regions.[20] This means that the measured field is effectively the field radiated by the tip, and recovering the details of the source at smaller radii will be difficult. On the other hand, if the aim is to accurately compute the acoustic field at a new set of points, it may well be sufficient to capture only the source at the tip.

The structure of the rotating field has been studied using model solutions,[21–23] and the role of the sonic radius has been clarified. The field is made up of a segmented near field, which undergoes a transition around r^*. In "tunneling" across this transition region, the sound field decays exponentially, explaining the relatively weak field radiated by subsonically rotating sources. Supersonic sources have part of the source lying beyond r^* so that they can radiate strongly into the field, without losing energy in tunneling through the transition. This transition region means that source recovery will always be a hard problem if only far-field data are available, a result which will be derived in Sec. II C by considering the bandwidth of the spatial data in the far field.

When the radiating system is a circular duct, the problem can be modeled by taking the noise source to be the duct termination. In that case, the source distribution is composed of the duct modes which have propagated to the end of the duct. The field inside a rigid circular duct is composed of modes of the form $J_n(k_{mn}r)\exp[j(n\theta - k_{zmn}z)]$, where $J_n(\cdot)$ is the Bessel function of the first kind, $J_n'(k_{mn})=0$, and k_{zmn} is an axial wavenumber.[14] When k_{zmn} has an imaginary part, the mode decays exponentially in the duct and does not propagate to the termination. In any case, the source strength at the duct termination can be taken to be the acoustic velocity generated by the modes which do propagate, and the radiated noise can be accurately computed over much of the field using a Rayleigh integral[3,14] or a Kirchhoff integral over a wider range of polar angles.[3,24] The source can again be modeled as a circular disk with an azimuthally varying source term. A number of methods have been developed for the identification of the radiating modes[2–6] and have been found to be accurate and robust, considering the assumptions made in their development.

The one extra difficulty in the duct case compared to the rotor problem is that the source at the duct termination may be composed of modes of more than one azimuthal order. In this case, there are procedures which use measurements at multiple angles to extract the modal amplitudes in the acoustic field. For example, a method has been presented which uses 360 measurements distributed over a semicircular "hoop" to find the amplitudes of the azimuthal modes radi-

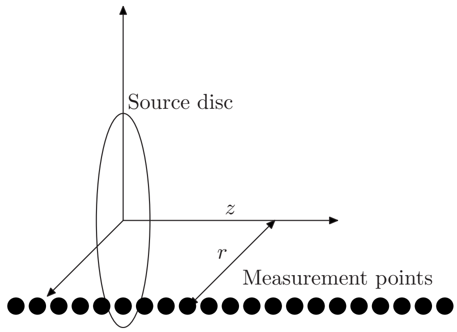

FIG. 2. Arrangement of experimental measurements.

ated from a duct.[2] The hoop of microphones was then moved to find the modal amplitudes as a function of axial displacement z.

From the known properties of rotating acoustic fields and established experimental techniques, it is clear that it is possible to measure and/or extract the complex amplitude of a single azimuthal mode radiated by a disk-shaped source. Indeed, if the source is tonal so that the modal content does not change with time, the measurements could, in principle, be performed with only two microphones, one fixed as a phase reference, and another moving along the sideline.

A. Formulation

Figure 2 shows the basic experimental arrangement. The input to the inversion method is the amplitude of a single azimuthal mode $p(r,z)$, with r fixed. When the sound is generated by a steady rotating source, $p(r,z)$ can be found by measuring the field on one sideline. When modes of different azimuthal order are present, the field must be measured on multiple sidelines of the same radius r, varying θ, and a decomposition procedure applied to find $p(r,z)$, as discussed in the previous section.

However the acoustic field may have been measured and processed, the sound radiated by one source mode of azimuthal order n at frequency ω is found by integration over the source disk,[12]

$$p(r,z) = \int_0^1 f(r_1) \int_0^{2\pi} \frac{e^{j(kR-n\theta_1)}}{4\pi R} d\theta_1 r_1 dr_1, \tag{3}$$

where the observer is positioned at $(r,0,z)$. The aim of the inversion algorithm is to recover the radial source distribution $f(r_1)$ from the field pressures $p(r,z)$.

To begin to recover $f(r_1)$, the first stage is to rewrite Eq. (3) in a transformed coordinate system (r_2,θ_2,z) centered on the measurement sideline (Fig. 3). This transformation has been used in calculations of transient radiation from pistons[13,25] and in studies of propeller noise fields.[21–23,26] Transforming Eq. (3) gives $p(r,z)$ as an integral over a line source $K(r,r_2)$,

$$p(r,z) = \int_{r-1}^{r+1} \frac{e^{jkR}}{R} K(r,r_2) r_2 dr_2, \tag{4}$$

$$R = (r_2^2 + z^2)^{1/2},$$

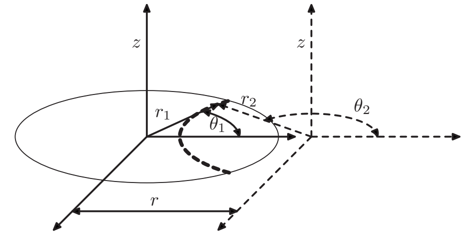

FIG. 3. Coordinate systems (r_1,θ_1,z) and (r_2,θ_2,z). The (r_2,θ_2,z) system is denoted by a dashed line, and the thick line shows the region of integration over θ_2 in the transformed system.

$$K(r,r_2) = \frac{1}{4\pi} \int_{\theta_2^{(0)}}^{2\pi-\theta_2^{(0)}} e^{-jn\theta_1} f(r_1) d\theta_2 \tag{5}$$

for observer positions with $r>1$. The original coordinates (r_1,θ_1) are related to (r_2,θ_2) by

$$r_1^2 = r^2 + r_2^2 + 2rr_2 \cos\theta_2, \tag{6a}$$

$$\theta_1 = \tan^{-1} \frac{r_2 \sin\theta_2}{r + r_2 \cos\theta_2}, \tag{6b}$$

so that the limits of integration in Eq. (5) are given by setting $r_1 = 1$,

$$\theta_2^{(0)} = \cos^{-1} \frac{1 - r^2 - r_2^2}{2rr_2}. \tag{7}$$

The function $K(r,r_2)$ depends only on the observer lateral displacement and is constant for all points on a sideline parallel to the source axis. The inversion method proposed is to measure $p(r,z)$ at fixed r, invert Eq. (4) to recover $K(r,r_2)$, and then use Eq. (5) to recover $f(r_1)$.

B. Inversion algorithm

The first stage of the inversion procedure is to use measured sideline data to recover the source function $K(r,r_2)$. Noting the behavior of K at its end points, Eq. (A3), we write

$$K(r,r_2) = [(r_2 - (r-1))(r+1-r_2)]^{1/2} K'(r,r_2). \tag{8}$$

The integral of Eq. (4) is discretized to give

$$\sum_{i=1}^{N} \frac{e^{jkR_{ij}}}{R_{ij}} (r + t_i^{(N)}) w_i^{(N)} K_i' = p_j, \tag{9}$$

where

$$R_{ij} = [(r + t_i^{(N)})^2 + z_j^2]^{1/2},$$

where z_j is the axial displacement of the jth measurement point and $(t_i^{(N)}, w_i^{(N)})$ are the nodes and weights of an N-point Gauss–Chebyshev quadrature rule of the second kind.

Equation (9) can be written as a system of equations relating the vector of measured pressures $\mathbf{p}$ to the unknown vector of sources $\mathbf{K}'$,

$$[\mathbf{A}]\mathbf{K}' = \mathbf{p}, \tag{10}$$

$$A_{ji} = \frac{e^{jkR_{ij}}}{R_{ij}}(r + t_i^{(N)})w_i^{(N)}. \tag{11}$$

In practice, the system will be overdetermined, with the number of measured pressures M being greater than N, the number of values of K' to be determined. At this stage, the system is solved for $\mathbf{K}'$, using some suitable method for ill-conditioned problems, with K being recovered from Eq. (8).

The second stage in determining the source distribution is to invert Eq. (5) to recover $f(r_1)$. We proceed by approximating $f(r_1)$ as a sum of Legendre polynomials $P_q(r_1)$,

$$f(r_1) = \sum_{q=0}^{Q} F_q P_q(r_1), \tag{12}$$

so that

$$K(r,r_2) = \frac{1}{4\pi}\sum_{q=0}^{Q} F_q \int_{\theta_2^{(0)}}^{2\pi-\theta_2^{(0)}} e^{-jn\theta_1} P_q(r_1)\,d\theta_2, \tag{13}$$

giving rise to the system of equations

$$[\mathbf{B}]\mathbf{F} = \mathbf{K}, \tag{14}$$

$$B_{iq} = \frac{1}{4\pi}\int_{\theta_2^{(0)}}^{2\pi-\theta_2^{(0)}} e^{-jn\theta_1} P_q(r_1)\,d\theta_2,$$

$$r_2 = r + t_i^{(N)}. \tag{15}$$

The integration is performed using a standard Gauss–Legendre quadrature. As before, this system can be solved using a method suitable for ill-conditioned problems and $f(r_1)$ reconstructed from the coefficient vector $\mathbf{F}$.

C. Far-field limitations

The integral of Eq. (4) is identical to the exact integral of Eq. (3). If we make the standard far-field approximations, we can establish some limit on the accuracy of reconstruction possible using far-field results. Expanding R to first order in r_2,

$$R \approx R_0 + \frac{r}{R_0}(r_2 - r), \quad R_0 = [r^2 + z^2]^{1/2},$$

so that

$$p \approx \frac{e^{jk(R_0 - r^2/R_0)}}{R_0}\int_{r-1}^{r+1} e^{jkrr_2/R_0} K(r,r_2) r_2\,dr_2, \tag{16}$$

which can be rewritten as

$$p \approx \frac{e^{jk(R_0 - r^2/R_0)}}{R_0}\int_{-\infty}^{\infty} e^{j\alpha r_2} K(r,r_2) r_2 H(r_2 - (r-1)) \times H(r + 1 - r_2)\,dr_2,$$

$$\alpha = kr/R_0, \tag{17}$$

where $H(\cdot)$ is the Heaviside step function.[27]

In the far field, Eq. (17) shows that the measured pressure on a sideline is proportional to a band-limited Fourier transform of the source term $K(r,r_2)$. A reconstruction algorithm based on far-field measurements can only recover components of $K(r,r_2)$ with spatial frequency $0 \leqslant \alpha \leqslant k$, with components outside this frequency band being lost in tunneling across the transition region between the near and far fields.

This result provides a link between NAH and the method of this paper. In NAH, a Fourier transform on the sideline data, i.e., Eq. (17), is used to recover the coefficients of a field expansion in cylindrical wave-functions.[17,18] This leads to difficulties with finite aperture effects due to the periodicity enforced by the finite Fourier transform. In this algorithm, no use is made of the Fourier transform in the reconstruction procedure so that the shortcomings of the finite Fourier transform do not cause the spurious sources which appear in NAH. On the other hand, the discretization introduced by the finite number of samples on the sideline can lead to aliasing as in NAH and any other reconstruction procedure based on spatial sampling of the acoustic field. The implication of Eq. (17) is that in order to use the information, which is present on the sideline, the sampling rate must be such as to capture behavior up to wavenumber k. If the minimum sampling rate is taken to be twice per wavelength, then the sideline measurements should be taken no more than π/k apart.

III. RESULTS

Two test cases have been simulated as a first test of the algorithm of Sec. II B. The first uses parameters characteristic of the counter rotating integrated shrouded propfan (CRISP) ducted rotor tests,[1] and the second models an automotive cooling fan which has been used in tests of noise control.[7,8] In each case, the sound field $p(z)$ is computed by integration of Eq. (3). To simulate measurement errors and background noise, a Gaussian random signal of amplitude $\epsilon \max|p|$ is added to the computed pressures before using them in the inversion scheme.

For the ducted rotor test case, M_t=0.74, k=7.4, n=10, M=128, N=64, r=1.125, and $0 \leqslant z \leqslant 4$. The source $f(r_1)$ was synthesized by adding the first four duct modes of circumferential order n with a random phase so that the source was given by

$$f(r_1) = \sum_{m=1}^{4} e^{j\phi_m} J_n(k_{mn} r_1),$$

where ϕ_m is a random phase $0 \leqslant \phi_m \leqslant 2\pi$. The number of measurement points M was chosen to be approximately equal to that in the CRISP tests where data were taken at 120 points.[1] Since the aim of the calculation was to assess the ability of the technique to resolve a source with multiple radial modes present, the modal amplitudes were kept equal and the phase randomized to generate an oscillatory source term.

In the cooling fan case, M_t=0.14, k=0.84, n=6, M=16, N=16, r=1.25, and $0 \leqslant z \leqslant 8$. This time, the source used was $f(r_1) = (1 - r_1)^{1/2}$, as this gives a reasonable physical behavior near the blade tip.[20] Again, the number of sensor positions

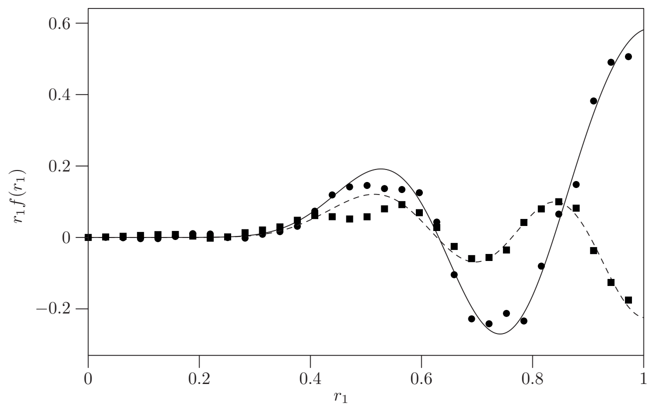

FIG. 4. Ducted fan test case, source term, $\epsilon=0$; solid and dashed lines, $\Re(f)$ and $\Im(f)$; circles and squares, $\Re(g)$ and $\Im(g)$.

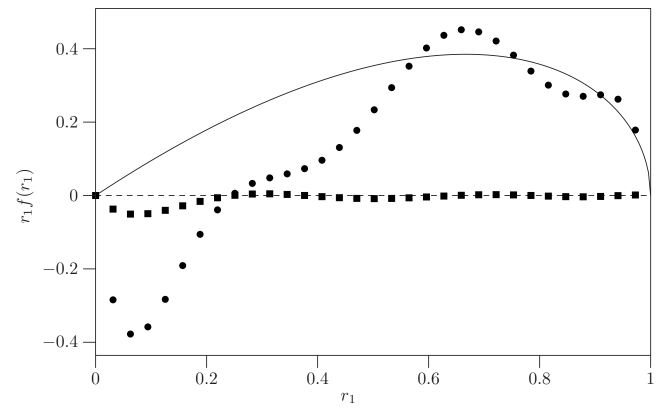

FIG. 6. Cooling fan test case, source term, $\epsilon=0$.

was chosen to be similar to that used in the original work: in this case, 17 microphones were used in the authors' source reconstruction experiments.[7,8]

The two test cases which have been chosen represent two realistic problems with quite different characteristics. The CRISP case is similar to many wind-tunnel tests which aim to extract the acoustic source from in-field measurements: the source is quite high frequency, and the tip Mach number is such that although energy is lost in the transition to the far field, the acoustic field is quite strong and there is sufficient information to allow the source to be determined reasonably accurately. The low-speed cooling fan, however, presents a rather more difficult problem. Due to the low rotor speed, the field decays rapidly inside the sonic radius $r^*=7.14$, and the measured field has lost much of the content useful for source reconstruction.

The inversion method has been implemented using OCTAVE (Ref. 28) and the REGULARIZATION TOOLS package of Hansen.[29,30] Equation (10) is solved using Hansen's implementation of truncated singular value decomposition,[31] with the regularization parameter automatically selected using the L-curve criterion.[32] The same technique is then used to solve Eq. (14) and to find $f(r_1)$.

Two measures are used to assess the accuracy of the method. The first is to compare the recovered source $g(r_1)$ with the input $f(r_1)$. The second is to use $g(r_1)$ to compute the acoustic field $q(r,z)$ at a new set of points and compare this field to $p(r,z)$ computed using $f(r_1)$. This assesses the ability of the algorithm to "project" measured data into the field.

A. Source reconstruction

The inversion algorithm has been run with zero added noise and with $\epsilon=10^{-3}$, equivalent to a maximum signal-to-noise ratio of 60 dB. Figures 4–7 show the reconstructed source for the two test cases, with the source terms weighted on radius r_1, as in the radiation integrals. The source reconstruction in the ducted fan case (Figs. 4 and 5) is quite good in both cases. With zero noise, it accurately reproduces the shape and amplitude of the input source. With added noise, the reconstruction is not quite as good, especially for inboard $r_1 \lessapprox 0.8$, but the details of the source are captured quite well near $r_1=1$, the dominant region for radiation at this wavenumber.

The cooling fan results (Figs. 6 and 7) are not as good, probably because the number of sensors is quite small and because the acoustic field is so much weaker than in the ducted fan case due to the low rotor speed. As discussed in Sec. II, sound from source regions inside the sonic radius decays exponentially as it radiates. Here the whole source lies inside the sonic radius, meaning that the acoustic field is composed largely of evanescent waves, making source reconstruction difficult.

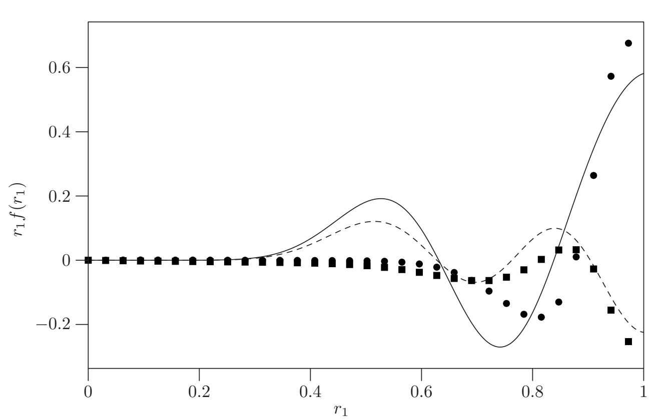

FIG. 5. Ducted fan test case, source term, $\epsilon=10^{-3}$.

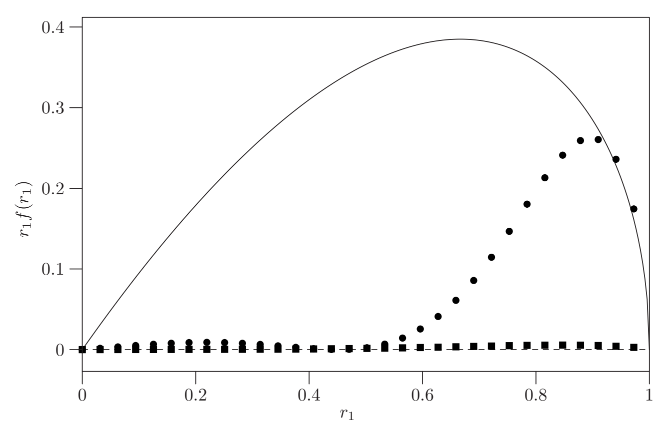

FIG. 7. Cooling fan test case, source term, $\epsilon=10^{-3}$.

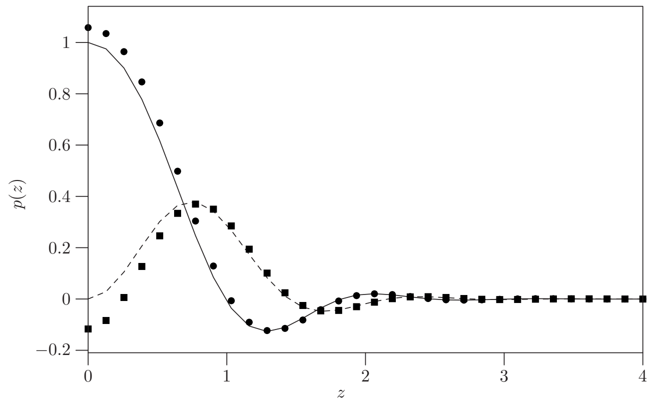

FIG. 8. Ducted fan test case, reconstructed near-field noise, $\epsilon=10^{-3}$: solid and dashed lines, $\Re(p)$ and $\Im(p)$; circles and squares, $\Re(q)$ and $\Im(q)$.

In Fig. 6, the reconstructed source oscillates considerably at small radii, but the tip behavior is very well captured. This might be expected: the tip is strongly dominant, meaning that the recovery of the inboard source is very poorly conditioned. With noise added, the reconstructed source is smoother, although the amplitude is not found accurately. The tip behavior, however, is again accurately computed.

B. Field estimation

Figures 8–12 compare the field computed using $g(r_1)$ to the real field $p(r,z)$, near $(r=2)$ and far from $(r=8)$ the source disk for the $\epsilon=10^{-3}$ case. The results have been scaled on $p(r,0)$ to simplify the comparison. Real and imaginary parts are shown separately as a check on the ability of the method to calculate the phase of the field, important in scattering calculations and in control.

The ducted fan results (Figs. 8 and 9) are very good. The phase has been accurately computed in the near and far fields, and the amplitude error is about 10% of the peak amplitude, or 1 dB. The directivity of the source is such that the field does not decay rapidly on the sideline, aiding the reconstruction technique. As a check that the method does converge to a correct result in the absence of noise, the reconstruction method has also been applied to data with $\epsilon=0$. The recomputed far-field pressures are shown in Fig. 10

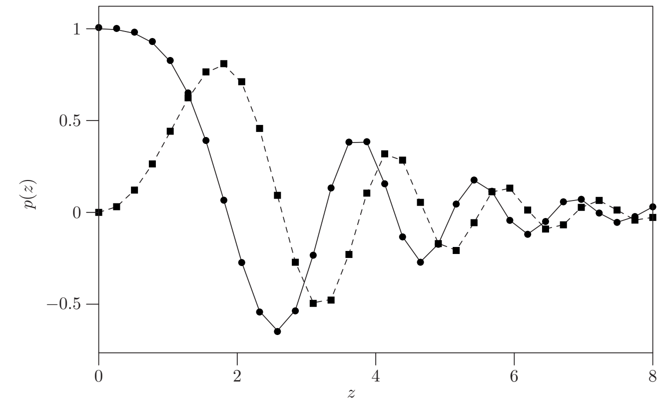

FIG. 10. Ducted fan test case, reconstructed far-field noise, $\epsilon=0$.

and, as they should be, are very close to the correct data, indeed practically indistinguishable from them with the amplitude error at $z=0$ being 0.06 dB.

In the cooling fan case (Figs. 11 and 12), the field decays rapidly and is reconstructed quite poorly. The shape and phase are roughly correct, but the amplitude error is about 50% or 4 dB. The error may be due to the form of the field or to the small number of sensors simulated. Note that although the amplitude of the reconstructed source is much less than that of $f(r_1)$, the reconstructed field amplitude is rather larger. This is due to the exponential dominance of the tip region as an acoustic source on subsonic rotors, mentioned in Sec. II: the difference in tip gradient for $g(r_1)$ has made the computed acoustic field stronger than that found using $f(r_1)$.

In any case, given that the phase has been accurately computed, the result might still be useful in control applications where the phase of the control signal is important in canceling the unwanted noise. Again, we present results with no added noise (Fig. 13), and, here, the comparison is not as good as in the ducted rotor case. The shape of the field has been well captured, but the amplitude is overestimated by about 3% or 0.26 dB.

C. Algorithm performance

To assess the performance of the method when used with varying numbers of measurements, the source reconstruction method has been applied to the simulated CRISP

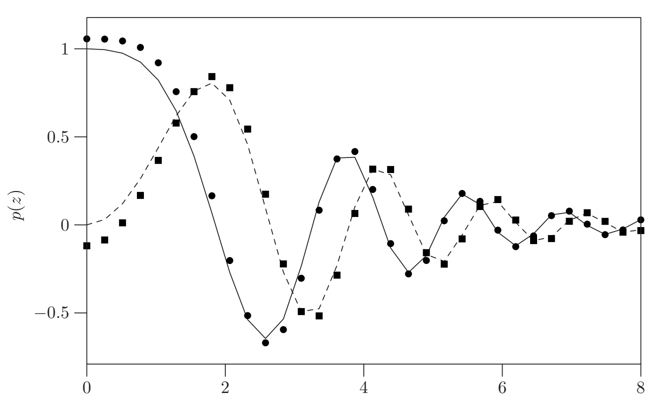

FIG. 9. Ducted fan test case, reconstructed far-field noise, $\epsilon=10^{-3}$.

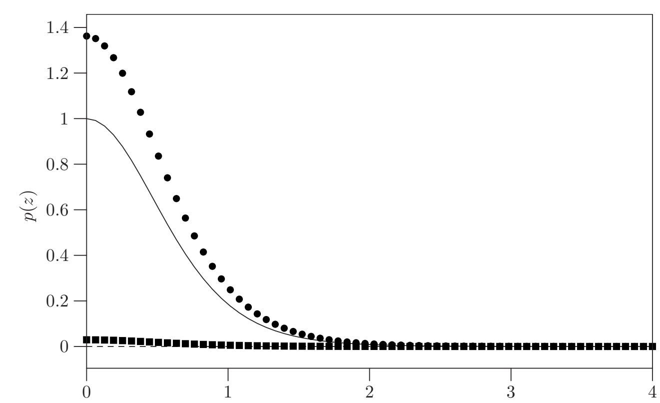

FIG. 11. Cooling fan test case, reconstructed near-field noise, $\epsilon=10^{-3}$.

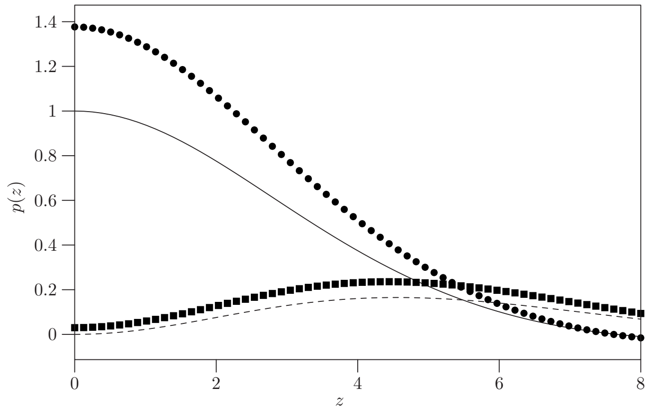

FIG. 12. Cooling fan test case, reconstructed far-field noise, $\epsilon=10^{-3}$.

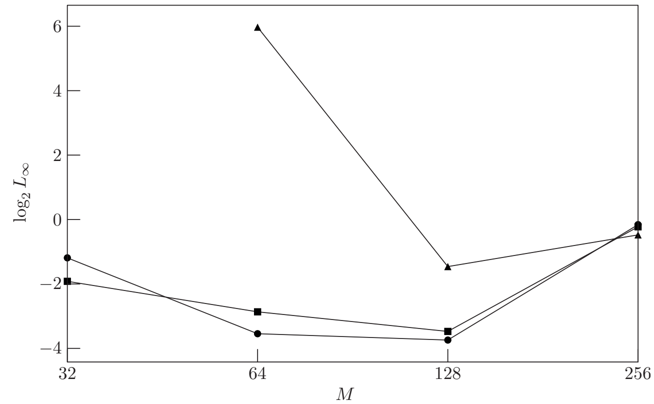

FIG. 14. Error ϵ vs number of sensor positions M and M/N. Squares: $M=N$; circles: $M=2N$; triangles: $M=4N$.

data with $M=32$, 64, 128, 256 and $M/N=1,2,4$. The error measure for the reconstructed source is the L_∞ norm,

$$L_\infty = \frac{\max|r_1 f(r_1) - r_1 g(r_1)|}{\max|r_1(f(r_1)\ |},$$

where the weighting with r_1 has been retained, corresponding to an area weighting of the error. The calculation has been performed with no added noise to check the factors which contribute to the error in the reconstructed quantities.

Figure 14 shows the variation in error with the number of sensors, as a function of the ratio M/N. The first obvious point is that for this set of operating parameters, the error for $M=64$ is very large when $M/N=4$, while the method failed completely at $M=32$. This appears to indicate that the source term cannot be well approximated by only $Q=16$ terms in the expansion of Eq. (12), an unsurprising result.

More interesting is that for $M/N=1,2$, the error decreases steadily as M increases but then increases between $M=128$ and $M=256$. Figure 15 shows the condition number κ of the matrices $[\mathbf{A}]$ and $[\mathbf{B}]$ used in the inversion procedure, as a function of M, with $N=M$. As might be expected, the condition number of both increases with M, as the systems become more poorly conditioned. Machine precision on the computer used for the calculations is approximately $1/2^{52}$. The condition number $\kappa(\mathbf{A})$ of the matrix used to estimate $K(r,r_2)$ is always greater than 2^{60} so that the first part of the inversion scheme is always ill conditioned. The reason for the drop in accuracy past $M=128$ seems to be the higher condition number of the second matrix used $\kappa(\mathbf{B})$. At $M=128$, it rises above 2^{52}, and we conjecture that at this point the loss of precision in calculations is too great for the inversion method and the results begin to worsen. This is a function of the solver used, and it may be that a different choice of regularization scheme would lead to better results.

IV. CONCLUSIONS

A source reconstruction method for the inversion of spinning acoustic fields has been developed and tested on two representative problems. It has been found that the method can work well, even with added noise, depending on the type of source to be identified. The method requires no *a priori* assumptions about the form of the source other than that it be circular and vary sinusoidally in azimuth. This makes it a useful intermediate between near-field acoustical holography, where no information is assumed about the source except its approximate location, and other source identification methods which use assumptions about the location and spatial variation of the source to model its radiation characteristics. In the case of the method of this paper, it may be that when additional information about the source is available, such as its modal structure, users might be able to incorporate this information into the technique to improve

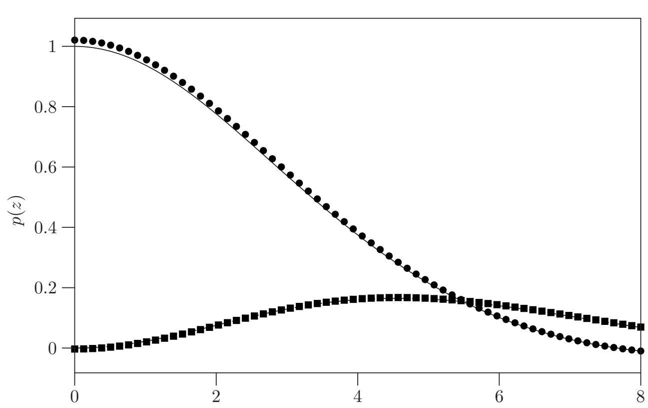

FIG. 13. Cooling fan test case, reconstructed far-field noise, $\epsilon=0$.

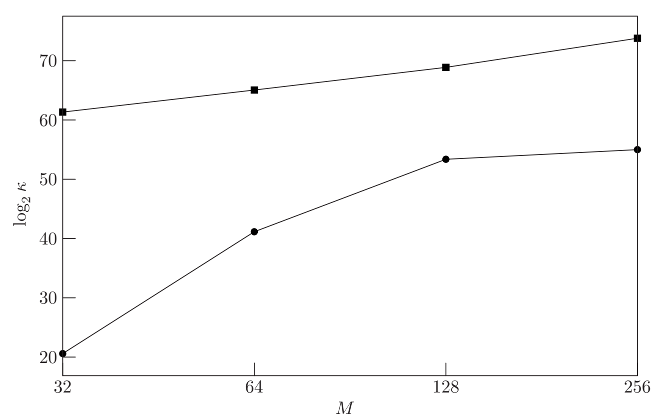

FIG. 15. Condition number κ of reconstruction matrices vs M, $N=M$. Squares: $[\mathbf{A}]$; circles: $[\mathbf{B}]$.

source reconstruction and/or to reduce the number of measurements required.

APPENDIX: END-POINT BEHAVIOR OF $K(r,r_2)$

To establish the behavior of $K(r,r_2)$ near the end points of the integrand in Eq. (4), we note that as $r_2 \to (r-1)$, $\theta_2^{(0)} \to \pi$ and $\theta_1 \to 0$. When $r_2 \to (r+1)$, $\theta_2^{(0)} \to \pi$ and $\theta_1 \to \pi$: We examine the basic integral,

$$K = \frac{1}{4\pi}\int_{\theta_2^{(0)}}^{2\pi-\theta_2^{(0)}} e^{-jn\theta_1} d\theta_2. \tag{A1}$$

For $\theta_2^{(0)} \to \pi$ and resulting small θ_1,

$$K \approx \frac{1}{4\pi}\int_{\theta_2^{(0)}}^{2\pi-\theta_2^{(0)}} 1 d\theta_2. \tag{A2}$$

Integrating,

$$K \approx (2\pi - 2\theta_2^{(0)})/4\pi$$

and using $\cos^{-1} x \to \pi-(1-x^2)^{1/2}$ as $x \to -1$ to give

$$\theta_2^{(0)} \approx \pi - \frac{2^{1/2}(r+1-r_2)^{1/2}(r_2-(r-1))^{1/2}}{(2rr_2)^{1/2}}$$

yields

$$K \approx \frac{(1+r-r_2)^{1/2}(r_2-(r-1))^{1/2}}{2(rr_2)^{1/2}}, \tag{A3}$$

with square root behavior as $r_2 \to (r-1)^+$ and $r_2 \to (r+1)^-$.

[1] F. Holste and W. Neise, "Noise source identification in a propfan model by means of acoustical near field measurements," J. Sound Vib. **203**, 641–665 (1997).
[2] F. Farassat, D. M. Nark, and R. H. Thomas, "The detection of radiated modes from ducted fan engines," in the Seventh AIAA/CEAS Aeroacoustics Conference, American Institute of Aeronautics and Astronautics, Maastricht (2001), Paper No. AIAA 2001-2138.
[3] S. Lewy, "Inverse method predicting spinning modes radiated by a ducted fan from free-field measurements," J. Acoust. Soc. Am. **117**, 744–750 (2005).
[4] S. Lewy, "Numerical inverse method predicting acoustic spinning modes radiated by a ducted fan from free-field test data," J. Acoust. Soc. Am. **124**, 247–256 (2008).
[5] F. O. Castres and P. F. Joseph, "Mode detection in turbofan inlets from near field sensor arrays," J. Acoust. Soc. Am. **121**, 796–807 (2007).
[6] F. O. Castres and P. F. Joseph, "Experimental investigation of an inversion technique for the determination of broadband duct mode amplitudes by the use of near-field sensor arrays," J. Acoust. Soc. Am. **122**, 848–859 (2007).
[7] A. Gérard, A. Berry, and P. Masson, "Control of tonal noise from subsonic axial fan. Part 1: Reconstruction of aeroacoustic sources from far-field sound pressure," J. Sound Vib. **288**, 1049–1075 (2005).
[8] A. Gérard, A. Berry, and P. Masson, "Control of tonal noise from subsonic axial fan. Part 2: Active control simulations and experiments in free field," J. Sound Vib. **288**, 1077–1104 (2005).
[9] N. Peake and W. K. Boyd, "Approximate method for the prediction of propeller noise near-field effects," J. Aircr. **30**, 603–610 (1993).
[10] P. Sijtsma, "Feasibility of noise source location by phased array beamforming in engine ducts," in the 13th AIAA/CEAS Aeroacoustics Conference, American Institute of Aeronautics and Astronautics, Rome (2007), Paper No. AIAA 2007-3696.
[11] C. R. Lowis and P. Joseph, "A focused beamformer technique for separating rotor and stator-based broadband sources," in the 12th AIAA/CEAS Aeroacoustics Conference, American Institute of Aeronautics and Astronautics, Cambridge (2006), Paper No. AIAA-2006-2710.
[12] M. Goldstein, "Unified approach to aerodynamic sound generation in the presence of solid boundaries," J. Acoust. Soc. Am. **56**, 497–509 (1974).
[13] A. D. Pierce, *Acoustics: An Introduction to Its Physical Principles and Applications* (Acoustical Society of America, New York, 1989).
[14] J. M. Tyler and T. G. Sofrin, "Axial flow compressor noise studies," SAE Trans. **70**, 309–332 (1962).
[15] J. W. Posey, M. H. Dunn, and F. Farassat, "Quantification of inlet impedance concept and a study of the Rayleigh formula for noise radiation from ducted fan engines," in the Fourth AIAA/CEAS Aeroacoustics Conference, American Institute of Aeronautics and Astronautics, Toulouse (1998), Paper No. AIAA 98-2248.
[16] M. B. S. Magalhães and R. A. Tenenbaum, "Sound sources reconstruction techniques: A review of their evolution and new trends," Acta Acust. **90**, 199–220 (2004).
[17] E. G. Williams, *Fourier Acoustics: Sound Radiation and Nearfield Acoustical Holography* (Academic, London, 1999).
[18] E. G. Williams, H. D. Dardy, and K. B. Washburn, "Generalized nearfield acoustical holography for cylindrical geometry: Theory and experiment," J. Acoust. Soc. Am. **81**, 389–407 (1987).
[19] D. G. Crighton and A. B. Parry, "Asymptotic theory of propeller noise. Part II: Supersonic single rotation propeller," AIAA J. **29**, 2031–2037 (1991).
[20] A. B. Parry and D. G. Crighton, "Asymptotic theory of propeller noise. Part I: Subsonic single rotation propeller," AIAA J. **27**, 1184–1190 (1989).
[21] C. J. Chapman, "The structure of rotating sound fields," Proc. R. Soc. London, Ser. A **440**, 257–271 (1993).
[22] M. Carley, "Sound radiation from propellers in forward flight," J. Sound Vib. **225**, 353–374 (1999).
[23] M. Carley, "Propeller noise fields," J. Sound Vib. **233**, 255–277 (2000).
[24] S. T. Hocter, "Exact and approximate directivity patterns of the sound radiated from a cylindrical duct," J. Sound Vib. **227**, 397–407 (1999).
[25] F. Oberhettinger, "On transient solutions of the 'baffled piston' problem," J. Res. Natl. Bur. Stand., Sect. B **65**, 1–6 (1961).
[26] M. Carley, "The structure of wobbling sound fields," J. Sound Vib. **244**, 1–19 (2001).
[27] M. J. Lighthill, *An Introduction to Fourier Analysis and Generalised Functions* (Cambridge University Press, Cambridge, 1958).
[28] J. W. Eaton, OCTAVE, http://www.octave.org (Last viewed November 3, 2008).
[29] P. C. Hansen, "Regularization Tools: A Matlab package for analysis and solution of discrete ill-posed problems," Numer. Algorithms **6**, 1–35 (1994).
[30] P. C. Hansen, "Regularization Tools version 4.0 for Matlab 7.3," Numer. Algorithms **46**, 189–194 (2007).
[31] P. C. Hansen, "Regularization Tools: A Matlab package for analysis and solution of discrete ill-posed problems," Technical report, Technical University of Denmark, www.netlib.org/numeralgo (Last viewed November 3, 2008).
[32] P. C. Hansen and D. P. O'Leary, "The use of the L-curve in the regularization of discrete ill-posed problems," SIAM J. Sci. Comput. (USA) **14**, 1487–1503 (1993).